Computational Materials Science 95 (2014) 228–234

Contents lists available at ScienceDirect

Computational Materials Science

journal homepage: www.elsevier.com/locate/commatsci

First-principles investigation of elastic and thermodynamic properties of SiCN under pressure

Jinhuan Jia [a], Dawei Zhou [a], Jie Zhang [b], Feiwu Zhang [c,d], Zhiwen Lu [a], Chunying Pu [a,*]

[a] College of Physics and Electronic Engineering, Nanyang Normal University, Nanyang 473061, China
[b] Department of Electrical and Electronic Engineering, Xian Jiaotong Liverpool University, Xian 215123, China
[c] Nanochemistry Research Institute, Curtin University, Perth, WA 6845, Australia
[d] State Key Laboratory of Ore Deposit Geochemistry, Institute of Geochemistry, Chinese Academy of Sciences, Guiyang 550002, China

ARTICLE INFO

Article history:
Received 31 May 2014
Received in revised form 23 July 2014
Accepted 26 July 2014
Available online 13 August 2014

Keywords:
SiCN
First-principles
Elastic constants
Elastic anisotropy

ABSTRACT

The structural and thermodynamic properties of the hexagonal, tetragonal, and orthorhombic phases of SiCN under high pressure are investigated by first-principles study based on the pseudo-potential plane-wave density functional theory method. The calculated equilibrium lattice constants, bulk modulus and elastic constants at zero pressure agree well with the previous theoretical values. The t-SiCN exhibits an indirect band gap with a value of 1.67 eV. It is found that with increasing pressure, the Debye temperature Θ_D of the o-SiCN and h-SiCN increase, whereas the one of the t-SiCN decreases. Furthermore, the o-SiCN is found to be a brittle material up to 60 GPa, while for t-SiCN and h-SiCN, the change from the brittle to ductile state occurs at about 17.04 GPa and 40.55 GPa, respectively. The calculated anisotropy factors demonstrate that both the o-SiCN and h-SiCN have a weak anisotropy up to 60 GPa, while the t-SiCN exhibits a high degree of anisotropy in shear but only a small anisotropy in compressibility. The ideal tensile and shear strength at large strains of the three phases are examined to further understand the microscopic mechanism of the structural deformation. It is found that all the SiCN compounds have a low ideal strength within 40 GPa, revealing that they may not be intrinsically superhard.

© 2014 Published by Elsevier B.V.

1. Introduction

The synthesis of silicon carbon nitride (SiCN) alloys has attracted much attention for its excellent chemical and physical properties. These compounds have high good creep properties, thermal shock resistance, and excellent oxidation resistance over a broad temperature range. Especially, since the short chemical bonds can be formed among the Si, C, and N atoms [1,2], the silicon carbon nitride (SiCN) alloys were expected to be a new kind of superhard materials [3–5]. Thus the synthesizing processes of SiCN compounds are growing rapidly [6–14]. Two crystalline solids, the cubic SiC_2N_4 with space group Pn3 m and the orthorhombic Si_2CN_4 with space group Aba2 were synthesized at ambient in 1997 [8]. However, the calculated Vickers hardness (H_V) values of the cubic and orthorhombic compounds are only 16.9 and 28.2 GPa, respectively [15]. The long linear Si−N=C=N−Si fragments are believed to limit the hardness of these materials. To address the issue, the Si−C−N films were synthesized successfully to improve the hardness of that material.

High-pressure synthesis is another important method to synthesize new Si−C−N superhard materials. For example, Wang et al. [15] explored the high-pressure structures of SiC_2N_4 and Si_2CN_4 using ab initio evolutionary simulations with the USPEX code [16–18]. They discovered novel structures of monoclinic C2/m and orthorhombic Cmmm for SiC_2N_4 and monoclinic C2/m and $P2_1/m$ structures for Si_2CN_4. Moreover, they found that the Cmmm SiC_2N_4 and C2/m and $P2_1/m$ Si_2CN_4 are potential superhard materials using hardness calculations; all of them have a hardness value exceeding 50 GPa. Very recently, Cui et al. [19] performed an extensive structural search of SiCN compounds using crystal structure analysis by particle swarm optimization (CALYPSO) algorithm [20]. They reveal that the new discovered tetragonal SiCN (t-SiCN) was energetically stable than the c-SiCN proposed 40 years ago [21], and two high-pressure phases of orthorhombic SiCN (o-SiCN) and hexagonal SiCN (h-SiCN) were also predicted. Transformations from t-SiCN to o-SiCN and h-SiCN occurred at 21.6 and 21.9 GPa, respectively. The h-SiCN and o-SiCN were believed to can be quenched at ambient conditions and exist in metastable phases. The hardness of t-SiCN, o-SiCN and h-SiCN were calculated to be 41.5, 30.0, and 30.2 GPa, respectively [19]. For superhard materials, it is necessary to examine the pressure influences on its elastic

* Corresponding author.
E-mail address: puchunying@126.com (C. Pu).

http://dx.doi.org/10.1016/j.commatsci.2014.07.044
0927-0256/© 2014 Published by Elsevier B.V.

stiffness and thermodynamic properties. Up to now, the microscopic mechanism of the structural deformation, the elastic properties and thermodynamic properties of the new discovered SiCN under pressure have not been investigated. The investigations on above issues are very important to extend our knowledge to material's performance under extremely severe environment, and also may provide important information for the potential applications of the crystals once they are synthesized. Thus in the present works, we have performed first principles calculations of the electronic structure, strain–stress behavior, elastic and thermodynamic properties for the three phases of SiCN. The Debye temperature, the ductile or brittle characters and elastic anisotropy of SiCN under pressure are discussed in detail.

2. Theoretical method

The calculations in this work are performed using CASTEP code [22,23] which is based on density functional theory. The exchange–correlation effects were taken into account within the Perdew–Burke–Ernzerhof (PBE) [24] scheme in the generalized gradient approximation (GGA) pseudopotential [25]. To describe interactions between electrons and core ions, the Vanderbilt ultrasoft pseudopotentials [26] were used. Pseudo atomic calculations are performed for Si: $3s^2 3p^2$, C: $2s^2 2p^2$ and N: $2s^2 2p^3$. The electronic wave function was expanded in a plane-wave basis set with a well converged cutoff energy of 500 eV for all cases. The k point separation in Brillouin zone of the reciprocal space was 0.03 $Å^{-1}$. The tolerances for the geometry optimization were: difference in total energy within 5×10^{-6} eV/atom, maximum ionic Hellmann–Feynman force within 0.01 eV/Å, maximum ionic displacement within 5×10^{-4} Å and maximum stress within 0.02 GPa. The quasi static ideal strength was determined using a method described previously [27]. The lattice vectors were incrementally deformed in the direction of the applied strains. At each step, the atomic basis and all the atoms inside the unit cell were simultaneously relaxed unit all the components of the Hellmann–Feynman stress tensor orthogonal to the applied strains were less than 0.1 GPa.

3. Results and discussion

3.1. Formation enthalpy and the structural parameters

In this work, three phases of SiCN predicted by Cui et al. [19] with hexagonal symmetry (h-SiCN, with space group of R3m), tetragonal symmetry (t-SiCN, with space group of P42nm), and orthorhombic symmetry (o-SiCN, with space group of Pnma) were investigated. As can been seen from Fig. 1, h-SiCN, t-SiCN and o-SiCN have 3, 4 and 4 SiCN formula units in their conventional cell, respectively. The enthalpy differences between t-SiCN and o-SiCN relative to h-SiCN as a function of pressure are calculated and shown in Fig. 2. The transformations from t-SiCN to o-SiCN and h-SiCN occurr at 17.1 and 18.0 GPa, respectively, which are little smaller than the values of 21.6 and 21.9 GPa in previous work [19]. The difference might result from the ultrasoft-potential used in our case instead of the norm-conserving pseudopotentials. The calculated equilibrium lattice constants, the bulk modulus (B), elastic constants and the shear modulus (G) of h-SiCN, t-SiCN, and o-SiCN at zero pressure are given in Table 1. It can be seen that all the calculated values are in good agreement with the previous results [19], indicating our calculations are valid and believable.

3.2. The band structure and Mulliken population analysis

In the previous work, t-SiCN was reported to be an intrinsic semiconductor with a band gap of 0.89 eV using the density function theory (DFT) [19]. In fact, superhard materials are often found to be wide-band semiconductors. However, it is known that DFT underestimates the gap energies of semiconductor, therefore we recalculated the band structure and the corresponding total density of states of t-SiCN along the high symmetry directions using the more accurate HSE hybrid density functional theory [28,29] as shown in Fig. 3. It can be seen that t-SiCN is an indirect band-gap semiconductor with the valence band maximum at the A-point and the conduction band minimum at Z-point. The band gap is calculated to be about 1.67 eV, which is higher than 0.89 eV from DFT calculation. Unfortunately, no experimental data of the band gap values are available for our comparison. We hope our results can be served as a prediction for the future experimental investigations.

We also performed the Mulliken populations analysis [30] (shown in Table 2) to reveal the bonding situation in those SiCN materials under pressure. For all three phases, a charge transfer from Si to C and N atoms is observed, and the Si-s orbital and Si-p orbital loose charge, transferring it to C-p orbital and N-p orbital. Charge transfer from Si to N are higher than that of Si—C, implying the strong bonding nature between Si and N in the three phases at 0 GPa. The bond character in mainly determined by Si—C and Si—N. As pressure increases, the total charges of Si in the three phases of SiCN all decrease by about 0.08, implicating the components of covalent bond increase. Furthermore, with pressure increasing, the charge transfer from Si to C in t-SiCN and and o-SiCN is higher than that of Si—N, which means the strong bonding character between Si and C. However, the charge transfer from Si to C is equal to Si to N in h-SiCN.

3.3. The elastic constants and elastic properties

The elastic constant is essential for many applications related to the mechanical properties of a solid material, especially for superhard materials. In general, the elastic constant C_{ij} tensor can be expressed (in abbreviated form) in a 6×6 square matrix, with 36 components. Due to the structure symmetry, the maximum number of independent parameters can be reduced. For hexagonal, tetragonal and orthorhombic phases, there are five, six and nine independent elastic constants, respectively. The mechanical stability criteria for the hexagonal, tetragonal and orthorhombic phase are given below:

Hexagonal structure [31]:

$$C_{44} > 0, \quad C_{11} > |C_{12}|, \quad (C_{11} + 2C_{12})C_{33} > 2C_{13}^2 \tag{1}$$

Tetragonal structure [32]:

$$\begin{aligned} &C_{11} - C_{12} > 0, \quad C_{11} + C_{33} - 2C_{13} > 0, \quad C_{11} > 0, \quad C_{33} > 0 \\ &C_{44} > 0, \quad C_{66} > 0, \quad 2C_{11} + C_{33} + 2C_{12} + 4C_{13} > 0 \end{aligned} \tag{2}$$

Orthorhombic structure [32]:

$$\begin{aligned} &C_{11} + C_{33} - 2C_{13} > 0, \quad C_{11} > 0, \quad C_{22} > 0, \quad C_{33} > 0, \quad C_{44} > 0, \\ &C_{55} > 0, \quad C_{66} > 0 \\ &C_{11} + C_{22} + C_{33} + 2C_{12} + 2C_{13} + 2C_{23} > 0 \\ &C_{11} + C_{22} - 2C_{12} > 0, C_{22} + C_{33} - 2C_{23} > 0 \end{aligned} \tag{3}$$

Fig. 4 presents the pressure dependence of elastic constants of SiCN for the three phases. All the elastic constants of the SiCN compounds satisfy the above conditions, which imply that they are mechanically stable up to 60 GPa. As we all know, the elastic constants C_{11} and C_{33} character the x- and z-direction resistance to linear compression, respectively. It is found that C_{11} and C_{33} are the largest among elastic constants for all the three phases, which indicate that all the three phases are very incompressible under

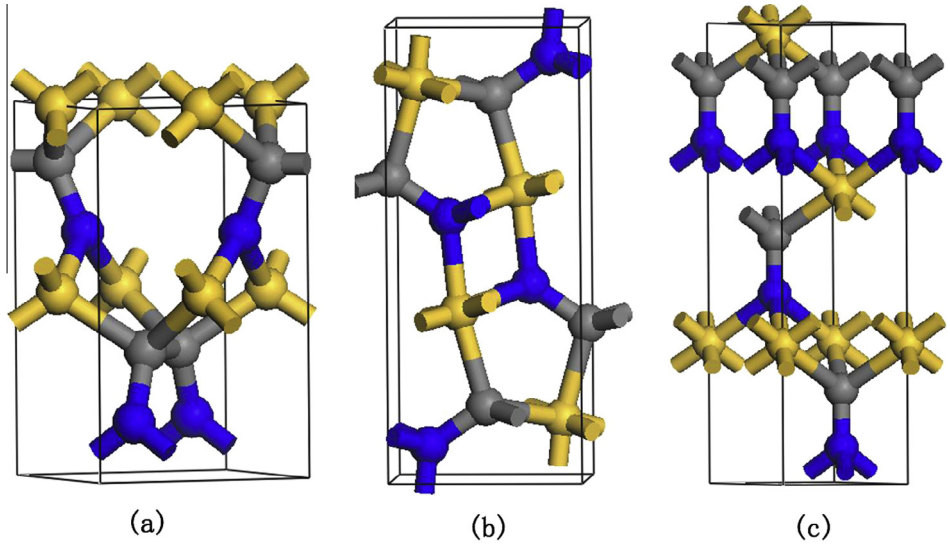

Fig. 1. Crystal structures of SiCN compounds at ambient pressure (a) t-SiCN, (b) o-SiCN, (c) h-SiCN. The Si, C, and N atoms are represented as yellow, grey and blue spheres, respectively. (For interpretation of the references to color in this figure legend, the reader is referred to the web version of this article.)

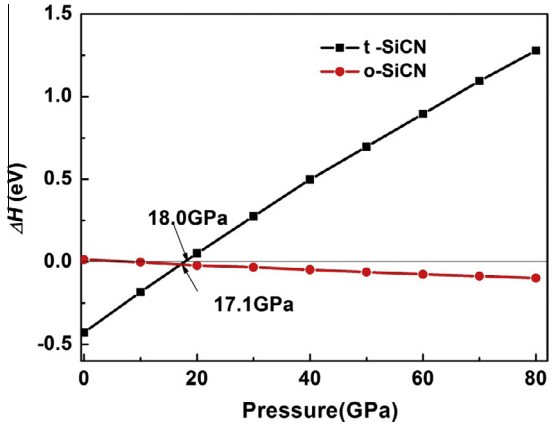

Fig. 2. Enthalpies of formation of different phases of SiCN as a function of pressure, where the h-SiCN is taken as the reference.

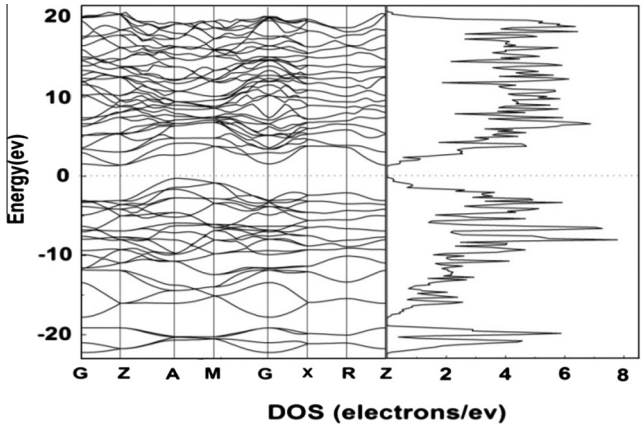

Fig. 3. Calculated band structure and density of state for t-SiCN. Energies are measured relative to the Fermi level (dash line).

Table 1
The calculated parameters *a*, *b*, and *c* (Å), bulk modulus *B* (GPa), elastic constants (GPa), shear modulus *G* (GPa) for SiCN compared with previous theoretical results at zero pressure.

	Hexagonal		Tetragonal		Orthorhombic	
	This work	Ref. [19]	This work	Ref. [19]	This work	Ref. [19]
a (Å)	2.860	2.834	4.108	4.069	9.159	9.080
b (Å)					2.754	2.729
c (Å)	10.509	10.429	6.836	6.788	3.892	3.861
C_{11}	393.3	411.2	329.4	340.8	601.5	624.9
C_{22}	–	–	–	–	378.2	393.0
C_{33}	956.1	1008.9	635.7	663.7	614.0	643.5
C_{44}	178.3	181.0	193.04	205.9	175.3	181.0
C_{55}	–	–	–	–	293.0	307.4
C_{66}	–	–	222.1	229.9	182.9	195.3
C_{12}	126.9	133.3	184.0	183.5	81.6	85.2
C_{13}	78.2	74.8	117.0	126.4	149.9	155.5
C_{23}	–	–	–	–	101.1	99.8
B	243	252	232	241	242	252
G	182	–	165	–	209	–

uniaxial stress along *x*- or *z*-axis. At the same time, we can find that C_{33} is higher than the C_{11} in the whole range of pressure for both h-SiCN and t-SiCN, indicating the *x* axis is more compressible than the *z* axis for these compounds, while the C_{11} and C_{33} of o-SiCN show similar trends at elevated pressures. It is notable that all elastic constants increase with increasing pressure except for the C_{44} in t-SiCN. The C_{44} of t-SiCN firstly increases with pressure, and then starts to decrease after 30 GPa. In the case of C_{44}, one can interpret that it indicates the resistances of the crystal with respect to the shear strain at (100) plane, and which is the important parameter relating to the shear modulus. So the C_{44} of t-SiCN is related to the decrease of shear modulus and Debye temperature as we will discuss later.

For bulk modulus, shear modulus and Young's modulus (*E*), they can be obtained by Voigt–Reuss–Hill (VRH) approximation [33]. The equations follow the Reuss and Voight definitions, the Hill values are defined as the arithmetic average of the Reuss and Voight values [34] (the minimum value for Reuss results and the maximum value for Voigt results):

$$B = (B_V + B_R)/2 \quad G = (G_V + G_R)/2 \quad E = \frac{9BG}{(3B+G)} \tag{4}$$

Hexagonal structure [35]:

$$C_{66} = (C_{11} - C_{12})/2 \tag{5}$$

Table 2
Mulliken populations of h-SiCN, t-SiCN and o-SiCN at 0 GPa and 30 GPa.

Structures	Pressure (GPa)	Elements	*s* (*e*)	*p* (*e*)	Total (*e*)	Charge (*e*)
Hexagonal	0	C	1.33	3.29	4.62	−0.62
		N	1.60	4.15	5.75	−0.75
		Si	0.93	1.70	2.63	1.37
	30	C	1.31	3.35	4.66	−0.66
		N	1.57	4.22	5.79	−0.79
		Si	0.85	1.70	2.55	1.45
Tetragonal	0	C	1.29	3.28	4.56	−0.56
		N	1.58	4.38	5.96	−0.96
		Si	0.91	1.56	2.47	1.53
	30	C	1.26	3.36	4.62	−0.62
		N	1.56	4.43	5.99	−0.99
		Si	0.84	1.54	2.39	1.61
Orthorhombic	0	C	1.35	3.24	4.59	−0.59
		N	1.60	4.16	5.76	−0.76
		Si	0.95	1.70	2.65	1.35
	30	C	1.33	3.31	4.64	−0.64
		N	1.57	4.22	5.80	−0.80
		Si	0.87	1.70	2.57	1.43

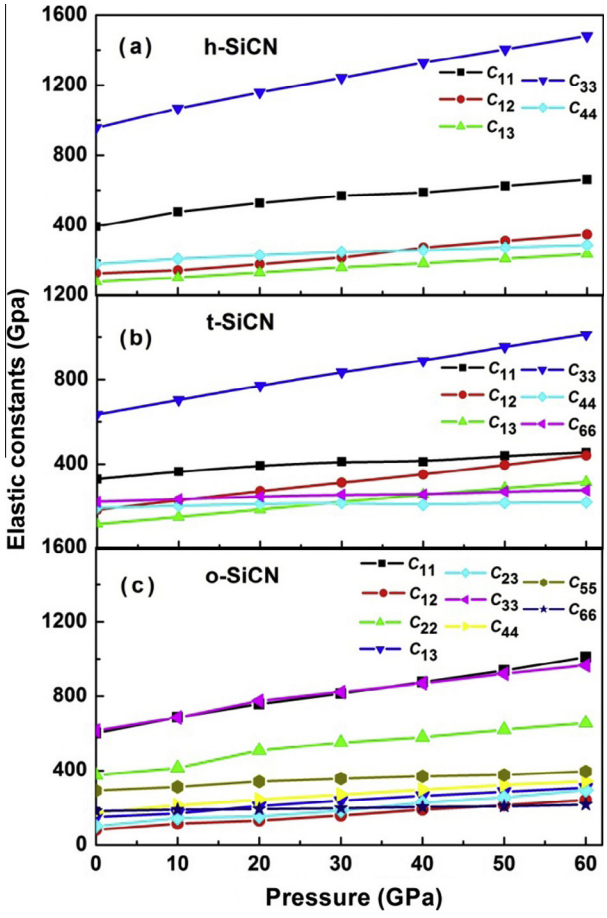

Fig. 4. Elastic stiffness constants of SiCN as a function of pressure.

$$B_V = \frac{1}{9}(2(C_{11}+C_{12})+C_{33}+4C_{13}) \tag{6}$$

$$B_R = \frac{(C_{11}+C_{12})C_{33}-C_{13}^2}{C_{11}+C_{12}+2C_{33}-4C_{13}} \tag{7}$$

$$G_V = \frac{1}{30}(C_{11}+C_{12}+2C_{33}-4C_{13}+12C_{44}+12C_{66}) \tag{8}$$

$$G_R = \frac{5}{2}\frac{\left[(C_{11}+C_{12})C_{33}-2C_{13}^2\right]^2 C_{44}C_{66}}{3B_V C_{44}C_{66}+\left[(C_{11}+C_{12})C_{33}-2C_{13}^2\right]^2(C_{44}+C_{66})} \tag{9}$$

Tetragonal structure [35]:

$$B_R = \frac{(C_{11}+C_{12})C_{33}-2C_{13}^2}{C_{11}+C_{12}+2C_{33}-4C_{13}} \tag{10}$$

$$B_V = \frac{1}{9}(2C_{11}+C_{33})+\frac{2}{9}(C_{12}+2C_{13}) \tag{11}$$

$$G_R = \frac{15}{18B_V/\left[(C_{11}+C_{12})C_{33}-2C_{13}^2\right]+6/(C_{11}-C_{12})+6/C_{44}+3/C_{66}} \tag{12}$$

$$G_V = \frac{1}{15}(2C_{11}+C_{33}-C_{12}-2C_{13})+\frac{1}{5}(2C_{44}+C_{66}) \tag{13}$$

Orthorhombic structure [36]:

$$B_V = \frac{1}{9}[C_{11}+C_{22}+C_{33}+2(C_{12}+C_{13}+C_{23})] \tag{14}$$

$$G_V = \frac{1}{15}[C_{11}+C_{22}+C_{33}+3(C_{44}+C_{55}+C_{66})-(C_{12}+C_{13}+C_{23})] \tag{15}$$

$$B_R = \Delta[C_{11}(C_{22}+C_{33}-2C_{23})+C_{22}(C_{33}-2C_{13})-2C_{33}C_{12} + C_{12}(2C_{23}-C_{12})+C_{13}(2C_{12}-C_{13})+C_{23}(2C_{13}-C_{23})]^{-1} \tag{16}$$

$$G_R = 15\{4[C_{11}(C_{22}+C_{33}+C_{23})+C_{22}(C_{33}+C_{13}) + C_{33}C_{12}-C_{12}(C_{23}+C_{12})-C_{13}(C_{12}+C_{13}) - C_{23}(C_{13}+C_{23})]/\Delta+3[(1/C_{44})+(1/C_{55})+(1/C_{66})]\}^{-1} \tag{17}$$

$$\Delta = C_{13}(C_{12}C_{23}-C_{13}C_{22})+C_{23}(C_{12}C_{13}-C_{23}C_{11}) + C_{33}(C_{11}C_{12}-C_{12}^2) \tag{18}$$

It can be seen from Fig. 5 that the bulk modulus of h-SiCN, t-SiCN and o-SiCN linearly increase monotonically when pressure is enhanced, while the shear modulus of the three phases exhibit different behavior. The shear modulus of o-SiCN increases with increasing pressure. While the shear modulus of h-SiCN first increases with pressure, then remains almost unchanged at higher

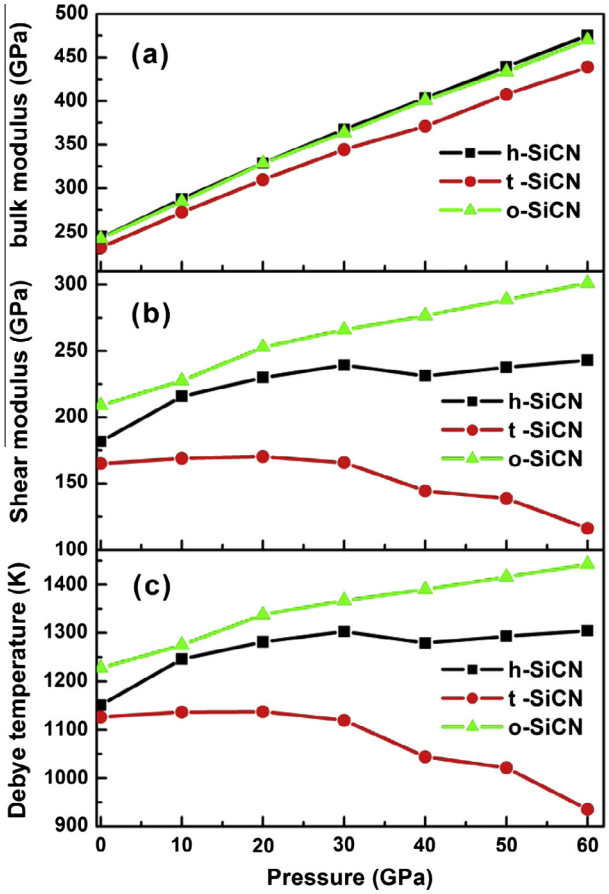

Fig. 5. Pressure dependence of the bulk modulus (B), shear modulus (G) and the Debye temperature (Θ_D) in hexagonal, orthorhombic, and tetragonal phases of SiCN.

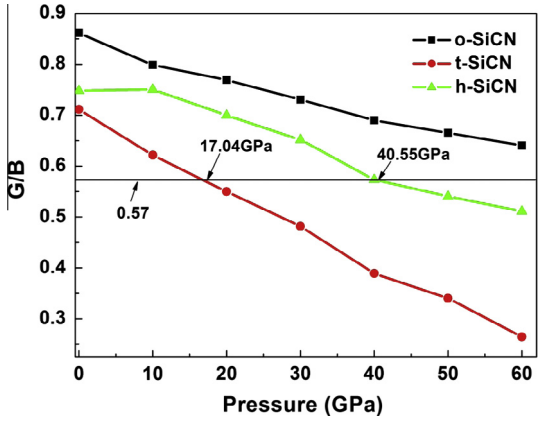

Fig. 6. G/B as a function of pressure.

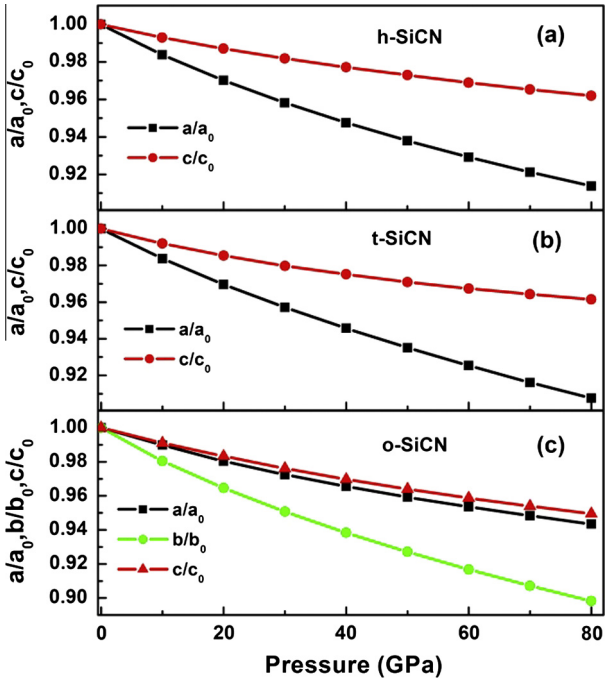

Fig. 7. a/a_0, b/b_0, and c/c_0 as a function of pressure.

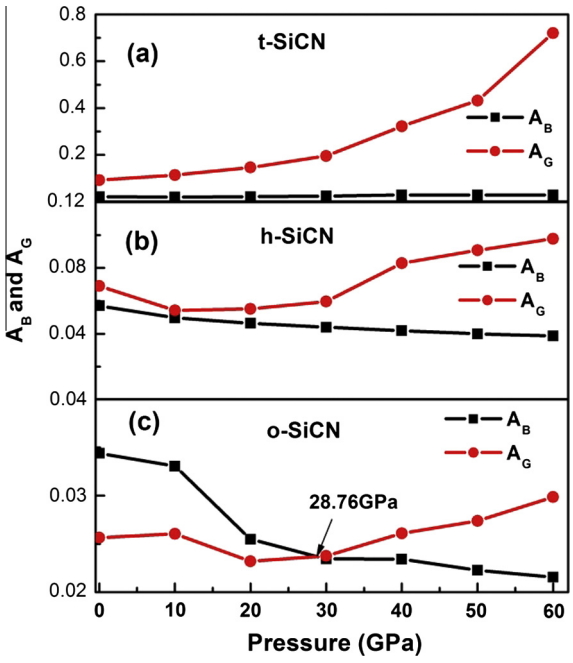

Fig. 8. The shear and compressibility anisotropy factors as a function of pressure.

pressure. Moreover, the shear modulus of t-SiCN is found to decrease at the pressure above 20 GPa, which have an important effect on its Debye temperature. As a fundamental parameter, the Debye temperature is linked to many physical properties of solids, such as melting point, thermal expansion, and Grüneisen [37]. The Debye temperature is defined in terms of the mean sound velocity v_m and gives explicit information about the lattice vibrations [38] and it is calculated using the equation [39]

$$\Theta_D = \frac{h}{k}\left[\frac{3n}{4\pi}\left(\frac{N_A\rho}{M}\right)\right]^{\frac{1}{3}} v_m \tag{19}$$

where h is Planck's constant, k is Boltzmann's constant, N_A is Avogadro's number, ρ is the density, M is the molecular weight and n is the number of atoms in the molecule. The average wave velocity is approximately calculated from [39]

$$v_m = \left[\frac{1}{3}\left(\frac{2}{v_s^3}+\frac{1}{v_l^3}\right)\right]^{-\frac{1}{3}} \tag{20}$$

where v_l and v_s are the longitudinal and transverse sound velocity, respectively, which can be obtained from following equations [40]

$$v_l = \sqrt{(B+4G/3)/\rho} \quad v_s = \sqrt{G/\rho} \tag{21}$$

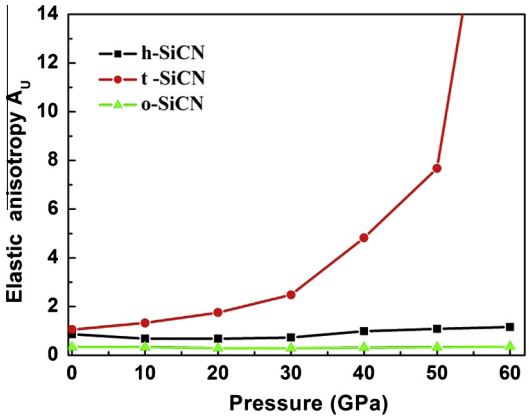

Fig. 9. Pressure dependence of the elastic anisotropy of SiCN.

From Fig. 5, it can be seen that the result of Debye temperature for SiCN is: o-SiCN > h-SiCN > t-SiCN. The pressure dependence of Θ_D in o-SiCN reveals almost a linear increase. The Θ_D of h-SiCN increases with increasing pressure and is nearly constant at high pressure, while the Θ_D of t-SiCN decreases significantly above 20 GPa. With increasing pressure, the changing trends of the Θ_D are almost the same as those of shear modulus in all three phases, implying shear modulus play an important role in determining the change of Θ_D with pressure.

To further predict the brittle and ductile behavior of solids, Pugh [41] introduced a simple relationship that the ratio of shear to bulk modulus (G/B) is associated with ductile or brittle characters of material. A high (low) G/B value is consistent with brittleness (ductility). The critical value which separates ductility from brittleness is about 0.57. The pressure effect on the G/B ratio of SiCN is shown in Fig. 6. It can be seen that the G/B ratio decreases with pressure for all the three phases. The G/B ratio of o-SiCN is larger than 0.57, implying the o-SiCN can be classified as a brittle material. The G/B ratio of t-SiCN and h-SiCN is equal to 0.57 at 17.04 GPa and 40.55 GPa, and thus the transition from the brittle to ductile state occurs at about 17.04 GPa and 40.55 GPa, respectively.

The elastic anisotropy of crystals has an important implication in engineering science since it is highly correlated with the possibility to induce microcracks in the materials [42]. We firstly investigate the anisotropy from the change of lattice parameters. All the a/a_0, b/b_0 and c/c_0 of three phases (where a_0, b_0 and c_0 are the zero pressure equilibrium structure parameters) have been calculated in pressure range of 0–80 GPa, which are illustrated in Fig. 7. As pressure increases, equilibrium ratio a/a_0 decreases more quickly than c/c_0 for both t-SiCN and h-SiCN, suggesting the compression along a-axis is larger. In addition, we also noticed that a/a_0 and c/c_0 almost exhibit the similar trends for o-SiCN, indicating the similar compressive ability for c-axis and a-axis.

A concept of percentage elastic anisotropy which is a measure of elastic anisotropy possessed by the crystal is proposed by Chung and Buessem[43]. The percentage anisotropy in compressibility and shear are defined as

$$A_B = \frac{B_V - B_R}{B_V + B_R} \quad A_G = \frac{G_V - G_R}{G_V + G_R} \tag{22}$$

where B and G are the bulk and shear modulus, and the subscripts V and R represent the Voigt and Reuss approximation. For these two expressions, a value of zero corresponds to complete elastic isotropy and a value of 100% means the maximum elastic anisotropy. As can be seen from Fig. 8, with increasing pressure, the anisotropy factor A_G of t-SiCN increases exponentially, while the anisotropy factor A_B remains constant. Therefore, t-SiCN exhibits relatively

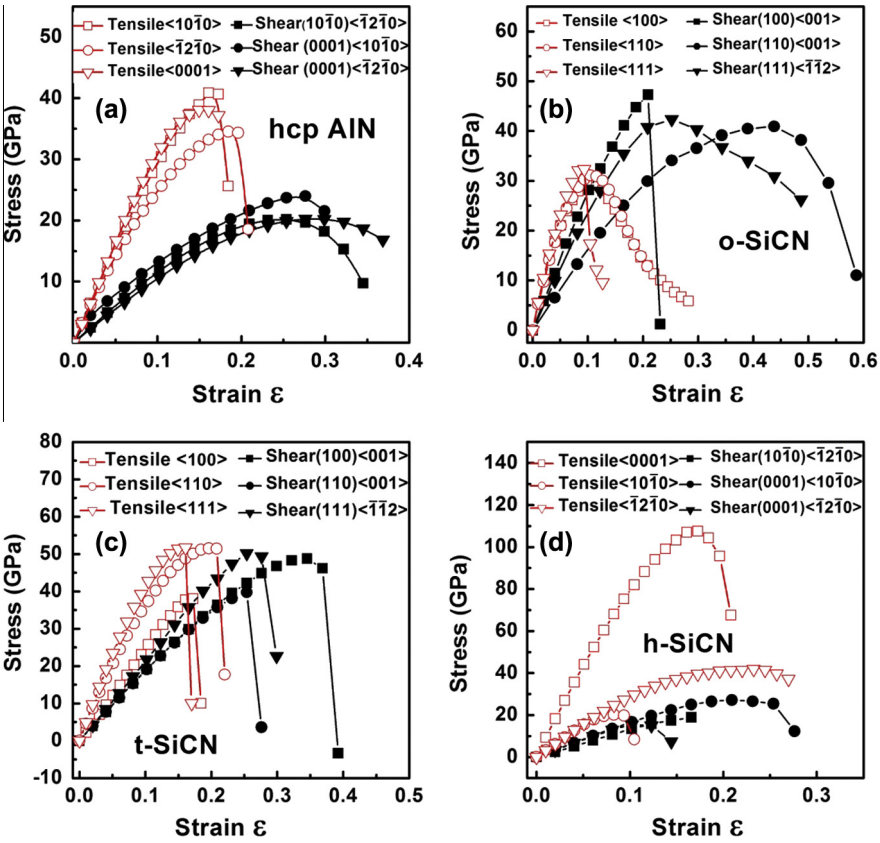

Fig. 10. The tensile stress–strain curves of hcp-AlN and the three SiCN compounds under tensile or shear load: (a) hcp-AlN, (b) o-SiCN, (c) t-SiCN and (d) h-SiCN.

high degree anisotropy in shear but only a small anisotropy in compressibility. For h-SiCN, the anisotropy factor A_B decreases with pressure, whereas the anisotropy factor A_G decreases firstly then increase after 10 GPa. The values of A_B and A_G are in the range of 3.9–5.7% and 5.4–9.8%, respectively. Clearly, the calculated anisotropy factors demonstrate that h-SiCN has a relatively small anisotropy. For o-SiCN, we can find that A_B is higher than A_G before 28.8 GPa. When the pressure exceeds 28.8 GPa, A_G starts to be higher than A_B. The values of A_B and A_G are in the range of 2.1–3.4% and 2.3–3.0%, respectively. It is considered that o-SiCN has a small anisotropy.

Alternatively, Ranganathan and Ostoja-Starzewshi [44] take into account both the shear and bulk contributions by recognizing the tensorial nature of the elastic stiffness instead of taking ratios of individual stiffness coefficients to define anisotropy. The universal anisotropy index that represents a measure to quantify the single crystal elastic anisotropy can be written as

$$A_U = 5\frac{G_V}{G_R} + \frac{B_V}{B_R} - 6 \tag{23}$$

For locally isotropic single crystals, A_U is identically zero. The departure of A_U from zero represents the extent of single crystal anisotropy. As can be seen from Fig. 9, the order of the elastic anisotropy is t-SiCN > h-SiCN > o-SiCN, hence the tetragonal phase is considered to have the maximum in elastic anisotropy among the three phases. The larger departure of A_U from zero is mainly due to the larger G_V/G_R. The values of A_U for h-SiCN are close to that of o-SiCN, showing a similar elastic anisotropy.

The ideal strength of a material is the stress at which the lattice itself becomes unstable and, hence, sets a firm upper bound on the mechanical strength the material can have. To assess the reliability of our computational approach, we first calculated the ideal strengths for hcp-AlN along different directions for tension and shear, which are shown in Fig. 10a, the ideal tensile and shear strength are about 35–40 and 20–22 GPa, respectively, in good agreement with the previous results [45]. Fig. 10b–d shows the stress–strain curves calculated for the three SiCN compounds. The ideal strengths for t-SiCN, o-SiCN and h-SiCN are calculated to be 37.7, 31.0 and 19.6 GPa respectively, suggesting that they may not be intrinsically superhard. Especially for h-SiCN, the maximum ideal strength is only about 19.6 GPa, the low ideal shear strength in $(0001)\langle 1\bar{2}10\rangle$ slip systems prevents it from becoming a superhard material.

4. Conclusions

The structural, electronic, elastic and thermodynamic properties as well as strain stress behavior of the hexagonal, tetragonal and orthorhombic SiCN under pressure have been investigated using the first-principles calculations. We found that the band structure of t-SiCN is characterized by an indirect transition of 1.67 eV using a more accurate HSE hybrid density functional theory. For the three SiCN compounds with increasing pressure, Si-s orbital and Si-p orbital loose charge, transferring mainly it to C-p orbital and N-p orbital. The calculated elastic constants reveal thatthe SiCN compounds meetthemechanically stability requirements up to 60 GPa. All the bulk modulus of h-SiCN, t-SiCN and o-SiCN increase linearly with the increasing pressure, while the shear modulus exhibit a different behavior. According to the values of G/B, it is found that o-SiCN is a brittle material, while for t-SiCN and h-SiCN, the transition from the brittle to ductile state occurs at about 17.04 GPa and 40.55 GPa, respectively. The calculated anisotropy factors demonstrate that o-SiCN and h-SiCN have a small anisotropy, while t-SiCN exhibits a high degree of anisotropy in shear but only a small anisotropy in compressibility. The ideal strengths for t-SiCN, o-SiCN and h-SiCN are calculated to be 37.7, 31.0 and 19.6 GPa respectively, revealing that they may not be intrinsically superhard. We hope that our results will stimulate further experimental study on those compounds.

Acknowledgements

This study is supported by Henan Joint Funds of the Natural Science Foundation of China (No. U1304612), the National Natural Science Foundation of China (Nos. 11247222 and 51374132), and Nanyang Normal University Science Foundation (Nos. ZX2013019 and ZX2012018).

References

[1] H.J. Du, D.C. Li, J.L. He, D.L. Yu, B. Xu, Z.Y. Liu, H.T. Wang, Y.J. Tian, Diamond Relat. Mater. 18 (2009) 72.
[2] A. Badzian, J. Am. Ceram. Soc. 85 (2002) 16–20.
[3] C.Z. Wang, E.G. Wang, Q.Y. Dai, J. Appl. Phys. 83 (1998) 1975–1978.
[4] J.E. Lowther, M. Amkreutz, T. Frauenheim, E. Kroke, R. Riedel, Phys. Rev. B 68 (2003) 033201.
[5] X.Y. Zhang, Z.W. Chen, H.J. Du, C. Yang, M.Z. Ma, J.L. He, Y.J. Tian, R.P. Liu, J. Appl. Phys. 103 (2008) 083533.
[6] L. An, R. Riedel, C. Konetschny, H.-J. Kleebe, R. Raj, J. Am. Ceram. Soc. 81 (1998) 1349–1352.
[7] R. Raj, L. An, S. Shah, R. Riedel, C. Fasel, H.-J. Kleebe, J. Am. Ceram. Soc. 84 (2001) 1803–1810.
[8] R. Riedel, A. Greiner, G. Miehe, W. Dressler, H. Fuess, J. Bill, F. Aldinger, Angew. Chem. Int. Ed. 36 (1997) 603–606.
[9] L.C. Chen, K.H. Chen, S.L. Wei, P.D. Kichambare, J.J. Wu, T.R. Lu, C.T. Kuo, Thin Solid Films 355–356 (1999) 112–116.
[10] A. Bendeddouche, R. Berjoan, E. Bêche, R. Hillel, Surf. Coat. Technol. 111 (1999) 184–190.
[11] L.C. Chen, C.K. Chen, S.L. Wei, D.M. Bhusari, K.H. Chen, Y.F. Chen, Y.C. Jong, Y.S. Huang, Appl. Phys. Lett. 72 (1998) 2463–2465.
[12] R. Machorro, E.C. Samano, G. Soto, L. Cota, Appl. Surf. Sci. 127–129 (1998) 564–568.
[13] X.M. He, T.N. Taylor, R.S. Lillard, K.C. Walter, M. Nastasi, J. Phys.: Condens. Matter 12 (2000) L591–L597.
[14] X.C. Xiao, Y.W. Li, L.X. Song, X.F. Peng, X.F. Hu, Appl. Surf. Sci. 156 (2000) 155–160.
[15] H.B. Wang, Q. Li, H. Wang, H.Y. Liu, T. Cui, Y.M. Ma, J. Phys. Chem. C 114 (2010) 8609–8613.
[16] J.E. Lowther, Phys. Rev. B 60 (1999) 11943–11946.
[17] H.J. Du, L.C. Guo, D.C. Li, D.L. Yu, J.L. He, Chin. Phys. Lett. 26 (2009) 016403.
[18] E. Betranhandy, L. Capou, S.F. Matar, Solid State Sci. 6 (2004) 315–323.
[19] L. Cui, Q.Q. Wang, B. Xu, D.L. Yu, Z.Y. Liu, Y.J. Tian, J.L. He, J. Phys. Chem. C 117 (2013) 21943–21948.
[20] Y.C. Wang, J. Lv, L. Zhu, Y.M. Ma, Phys. Rev. B 82 (2010) 094116.
[21] Inorganic Crystal Structure Database, <http://icsd.fiz-karlsruhe.de>, ICSD Collection Code 28391.
[22] S.J. Clark, M.D. Segall, C.J. Pickard, P.J. Hasnip, M.J. Probert, K. Refson, M.C. Payne, Z. Kristallogr. 220 (2005) 567–570.
[23] M.D. Segall, P.J.D. Lindan, M.J. Probert, C.J. Pickard, P.J. Hasnip, S.J. Clark, M.C. Payne, J. Phys.: Condens. Matter 14 (2002) 2717–2744.
[24] J.P. Perdew, K. Burke, M. Emzerhof, Phys. Rev. Lett. 77 (1996) 3865–3868.
[25] J.P. Perdew, J.A. Chevary, S.H. Vosko, K.A. Jackson, M.R. Pederson, D.J. Singh, C. Fiolhais, Phys. Rev. B 46 (1992) 6671–6687.
[26] D. Vanderbilt, Phys. Rev. B 41 (1990) 7892–7895.
[27] Q. Li, H.Y. Liu, D. Zhou, W.T. Zheng, Z.J. Wu, Y.M. Ma, Phys. Chem. Chem. Phys. 14 (2012) 13081–13087.
[28] J. Heyd, G.E. Scuseria, M. Ernzerhof, J. Chem. Phys. 124 (2006) 219906.
[29] J. Heyd, G.E. Scuseria, M. Ernzerhof, J. Chem. Phys. 118 (2003) 8207–8215.
[30] R.S. Mulliken, J. Chem. Phys. 23 (1995) 1833–1840.
[31] G.V. Sin'ko, N.A. Smirnow, J. Phys.: Condens. Matter 14 (2002) 6989–7005.
[32] O. Beckstein, J.E. Klepeis, G.L.W. Hart, O. Pankratov, Phys. Rev. B 63 (2001) 134112.
[33] J.P. Watt, J. Appl. Phys. 51 (1980) 1520–1524.
[34] R. Hill, Proc. Phys. Soc. London 65 (1952) 349–354.
[35] J.P. Watt, L. Peselnick, J. Appl. Phys. 51 (1980) 1525–1531.
[36] J.P. Watt, J. Appl. Phys. 50 (1979) 6290–6295.
[37] P. Ravindran, L. Fast, P.A. Korzhavyi, B. Johansson, J. Wills, O. Eriksson, J. Appl. Phys. 84 (1998) 4891–4904.
[38] A.M. Ibrahim, Nucl. Instrum. Methods Phys. Res., Sect. B 34 (1988) 135–136.
[39] O.L. Anderson, J. Phys. Chem. Solids 24 (1963) 909–917.
[40] E. Schreiber, O.L. Anderson, N. Soga, Mcgraw-Hill, New York, 1973.
[41] S.F. Pugh, Philos. Mag. 45 (1954) 823–843.
[42] V. Tvergaard, J.W. Hutchinson, J. Am. Ceram. Soc. 71 (1988) 157–166.
[43] D.H. Chung, W.R. Buessem, vol. 2, Plenum Press, New York, 1968, pp. 217–245.
[44] S.I. Ranganathan, M. Ostoja-Starzewski, Phys. Rev. Lett. 101 (2008) 055504.
[45] R.F. Zhang, S.H. Sheng, S. Veperk, Appl. Phys. Lett. 91 (2007) 031906.